ice
Institution of Civil Engineers
publishing

Bio- and Chemo-mechanical Processes in Geotechnical Engineering

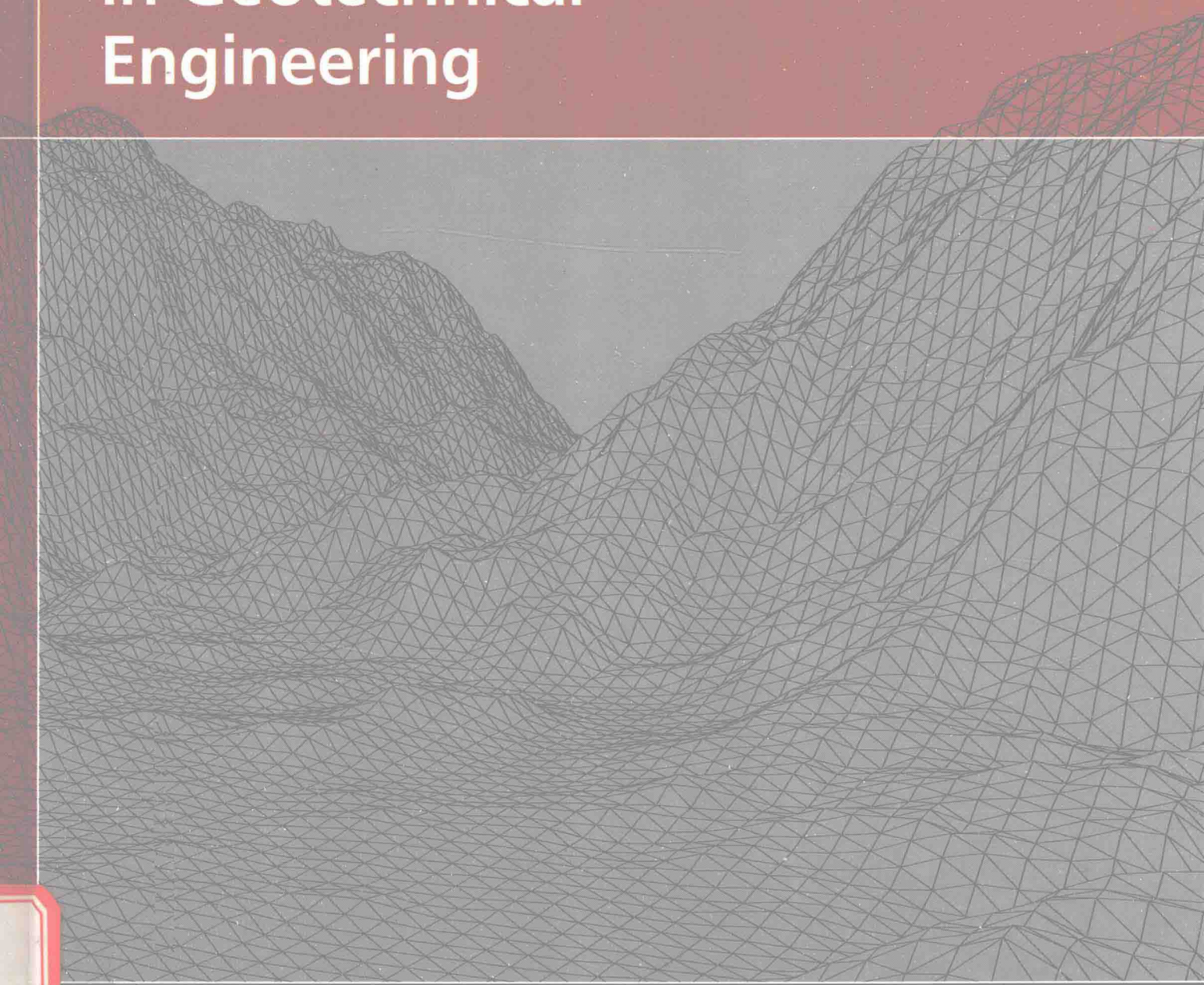

Edited by Lyesse Laloui

ice
Institution of Civil Engineers
publishing

Bio- and Chemo-Mechanical Processes in Geotechnical Engineering

Géotechnique Symposium in Print 2013

Edited by
Lyesse Laloui

ISBN 978-0-7277-6053-1

Typeset by Keytec Typesetting Ltd, Bridport, Dorset
Printed and bound by Ashford Colour Press Ltd, Gosport, Hants PO13 0FW

Preface

Conventional geotechnical engineering theories do not provide a sufficient framework to fully address the new challenges that emerge due to the interactions between multi-physical phenomena. During the past two decades, advances in the study of unsaturated geo-materials including the non-isothermal conditions have been reported. A whole new framework for the characterization of the coupled thermo-hydro-mechanical processes has been set. However, the complexity of emerging energy and environmental geotechnical applications is increasing with the presence and development of chemical and biological processes. The evolution of these phenomena and their interaction with the different constituents of porous geo-materials unfold a vast new research domain, full of challenges. This is leading the global scientific interest towards new areas, far from the conventional and extensively explored ones.

The objective of this book is to present the recent developments in the study of the aforementioned phenomena and to provide readers with a handful material for addressing the uncharted chemo- and bio- mechanical couplings and their related geotechnical applications.

In recent years, substantial advances have been made in understanding the coupling between chemical and biological processes and mechanical and hydraulic behaviour in soils and rocks. At the same time, experimentation and modelling capabilities have progressed significantly, allowing effective design of geotechnical applications. The need for such analyses arises (for example) in chemical and biological soil improvement; nuclear, hazardous and municipal waste containment; petroleum and natural gas extraction; methane hydrate exploitation; carbon dioxide sequestration; and the assessment of pavement durability.

In such areas, instances of complexity and interaction are many, mainly because of the coexistence of several constituents and phases, their interactions, their reactivity, and their often non-linear behaviour. Flow involves water and gas, including the transport of chemical species and bacteria. Geomaterial deformation depends not only on classical effective stress, suction and temperature, but also on the history of chemical and bacterial activity in the material. Experimental observations are often difficult to carry out, and laboratory and in situ tests are costly challenges. An understanding of the material behaviour to be observed requires the control or measurement of many different parameters. Modelling inevitably implies numerical analyses. Coupled transient analyses are in fact a characteristic feature of this field; proper variables must be selected which can describe the behaviour of the geomaterials subjected to chemical and biological phenomena.

A challenge at hand is to quantitatively describe the reaction and transport processes that occur. In this case, more complex variables enter the field equations for the different phases since the addressed chemical and biological processes refer to solute species that can react with species either in the same or in another phase. Robust numerical techniques are therefore required in order to solve, with sufficient accuracy, the strongly coupled analytical systems. Hence, progress in coupled bio- and chemo-mechanical processes in geotechnical engineering requires advances in theoretical formulations, numerical analyses, constitutive modelling and laboratory techniques, as well as detailed examination of well-documented field cases. Another issue is the study of the micro-structure where these processes can be better investigated and interpreted in mathematical terms. The analysis at the micro-scale requires the use of testing apparatus previously employed in limited cases in testing procedures for geotechnical problems.

This book is based on the two special issues of *Géotechnique* (Volume 63 issues 3 and 4) that preceded the *Géotechnique* Symposium in Print that was held on 3rd June 2013 at the Institution of Civil Engineers (ICE) in London. The symposium offered scientists and engineers from all over the world the opportunity to learn, discuss and outline future developments in this fascinating and critically important area. To this same purpose, the content of the book is enriched with papers from subsequent issues of the journal.

A total number of twenty contributions are organized in three sections. The first two focus on couplings between chemical, biological and mechanical aspects for different geo-materials (clay, shale, bentonite and sand among others) while emphasis is laid on modelling. Experimental evidence is presented along with cases addressing these couplings for real applications such as the mitigation of the liquefaction potential of sands or the carbon dioxide sequestration in coal beds. Finally, the third section is devoted to an overview of the progress in this emerging field providing at the same time readers with an outline of future challenges and potential developments.

Lyesse Laloui
Ecole Polytechnique Fédérale de Lausanne, EPFL
May 2014

Contents

Preface iii

Session 1. Chemo-mechanical investigations in soils

1.1 Clays

Double-structure effects on the chemo-hydro-mechanical behaviour of a compacted active clay 3
G. Musso, E. Romero and G. Della Vecchia

A chemo-mechanical constitutive model accounting for cation exchange in expansive clays 18
L. Do N. Guimarães, A. Gens, M. Sánchez and S. Olivella

An experimental and constitutive investigation on the chemo-mechanical behaviour of a clay 32
P. Witteveen, A. Ferrari and L. Laloui

Reduction of the clogging potential of clays: new chemical applications and novel quantification approaches 44
R. Zumsteg, M. Plötze and A. Puzrin

1.2 Other geo-materials

Coupled chemical-hydraulic-mechanical behaviour of bentonites 57
A. Dominijanni, M. Manassero and S. Puma

Environmentally enhanced crack propagation in a chemically degrading isotropic shale 72
M.M. Hu and T. Hueckel

A chemo-poro-mechanical model for sequestration of carbon dioxide in coalbeds 81
M.S. Masoudian, D.W. Airey and A. El-Zein

Growth of polymer microstructures between stressed silica grains: a chemo-mechanical coupling 90
R. Guo and T. Hueckel

Some unexpected effects of natural and anthropogenic chemicals on construction 99
S.A. Jefferis

Session 2. Bio-chemo-mechanical aspects in geomechanics

Effect of chemical treatment used in MICP on engineering properties of cemented soils 107
A. Al Qabany and K. Soga

Mitigation of liquefaction of saturated sand using biogas 116
J. He, J. Chu and V. Ivanov

Dynamic response of liquefiable sand improved by microbial-induced calcite precipitation 125
B.M. Montoya, J.T. Dejong and R.W. Boulanger

Volumetric consequences of particle loss by grading entropy [technical note] 136
J.R. McDougall, E. Imre, D. Barreto and D. Kelly

Session 3. Overview and future challenges

Biogeochemical processes and geotechnical applications: progress, opportunities and challenges 143
J.T. Dejong, K. Soga, E. Kavazanjian, S. Burns, L.A. Van Paassen, A. Al Qabany, A. Aydilek, S.S. Bang, M. Burbank, L.F. Caslake, C.Y. Chen, X. Cheng, J. Chu, S. Ciurli, A. Esnault-Filet, S. Fauriel, N. Hamdan, T. Hata, Y. Inagaki , S. Jefferis, M. Kuo, L. Laloui, J. Larrahondo, D.A.C. Manning, B. Martinez, B.M. Montoya, D.C. Nelson, A. Palomino, P. Renforth, J.C. Santamarina , E.A. Seagren, B. Tanyu, M. Tsesarsky and T. Weaver

Related content

Mathematical model of electro-osmotic consolidation for soft ground improvement 161
L. Hu and H. Wu

Analytical solution for axisymmetric electro-osmotic consolidation [technical note] 171
H. Wu and L. Hu

Improving the mechanical response of kaolinite and bentonite through exposure to organic and metallorganic compounds [technical note] 177
A. Gajo, A. Madaschi, F. Girardi and R. Di Maggio

Weathering of submerged stressed calcarenites: chemo-mechanical coupling mechanisms 183
M.O. Ciantia and T. Hueckel

Massive sulfate attack to cement-treated railway embankments 201
E.E. Alonso and A. Ramon

Microbial method for construction of an aquaculture pond in sand [technical note] 215
J. Chu, V. Ivanov, V. Stabnikov and B. Li

ice
Institution of Civil Engineers
publishing

Session 1. Chemo-mechanical investigations in soils

1.1 Clays

Musso, G. *et al.* (2013). *Géotechnique* **63**, No. 3, 206–220 [http://dx.doi.org/10.1680/geot.SIP13.P.011]

Double-structure effects on the chemo-hydro-mechanical behaviour of a compacted active clay

G. MUSSO*, E. ROMERO† and G. DELLA VECCHIA‡

This work presents an insight into double-structure effects on the coupled chemo-hydro-mechanical behaviour of a compacted active clay. In the first part, selected pore size distribution curves are introduced, to highlight the influence of solute concentration on the evolution of the microstructure of compacted samples. An aggregated structure with dual-pore network is induced by compaction even at relatively high water contents. This structural arrangement is enhanced by salinisation, and has a notable influence on transient volume change behaviour – that is, the occurrence of different stages of swelling upon pore water dilution and higher volume change rates upon salinisation. A coupled chemo-hydro-mechanical model, taking into consideration double-structural features from a chemo-mechanical viewpoint, is described and then used to interpret these behavioural responses and present complementary information on local transient processes. The model is designed to identify an intra-aggregate and an inter-aggregate domain, and assigns different values of hydraulic pressure and osmotic suction to each domain. Distinct constitutive laws for both domains are formulated, and the flow of salt and water between the two domains is accounted for by a physically based mass exchange term. The model is used to simulate salt diffusion tests run in an oedometer at constant vertical stress. Parameters used in the formulation are calibrated based on separate experimental evidence, both through direct test results and through back-analyses of laboratory experiments.

KEYWORDS: chemical properties; clays; constitutive relations; fabric/structure of soils; laboratory tests; suction

INTRODUCTION

The hydro-chemo-mechanical response of compacted active soils is of significant importance in geo-environmental engineering, such as for soil contamination/remediation and waste confinement at surface or at great depths using engineered clay barriers and clay liners (e.g. Delage & Romero, 2008). When designing compacted engineered clay barriers for waste repository systems, it is of primary importance to assess how hydraulic properties and the volume change response are affected by chemical changes induced by a wide range of saline concentrations and solute types.

Despite practical relevance for geo-environmental applications, not many studies have dealt with the effects of chemical changes on the volumetric behaviour of compacted and natural soils (e.g. Di Maio & Fenelli, 1997; Musso *et al.*, 2003; Rao *et al.*, 2006; Rao & Thyagaraj, 2007; Castellanos *et al.*, 2008; Siddiqua *et al.*, 2011), although chemo-mechanical interactions and pore fluid chemistry effects on reconstituted clays are a well-documented topic in the literature, and have a long research history (e.g. Bolt, 1956; Mesri & Olson, 1971a; Barbour & Fredlund, 1989; Yang & Barbour, 1992; Di Maio, 1996; Studds *et al.*, 1998).

The chemo-mechanical behaviour of slurries starting from diluted suspensions has historically been interpreted through Gouy–Chapman diffuse double layer (DDL) theory (e.g. Bolt, 1956; Warkentin *et al.*, 1957; Madsen & Muller-Vonmoos, 1985, 1989). This approach has been used to reproduce forces exchanged by particles in a system where the size of the pores is uniform (Mitchell & Soga, 2005). Despite being quite successful in explaining some features of the observed volumetric response, such as volume decrease upon salinisation, the hypothesis of a uniform pore size appears controversial when considering the behaviour of structured soils, and in general when considering hydraulic aspects.

For example, at a given void ratio, specimens saturated with saline solutions or with organic non-polar liquids show higher hydraulic conductivities than specimens saturated with distilled water (e.g. Michaels & Lin, 1954; Mesri & Olson, 1971a, 1971b; Fernandez & Quigley, 1985, Calvello *et al.*, 2005; Gajo & Maines, 2007). Hueckel *et al.* (1997) applied four different literature models to verify the impact of different mechanisms of microstructure evolution, induced by chemical changes, on the permeability of saturated active clays. They identified clusters of clay particles, saturated by immobile inter-layer water and external adsorbed water, as the fundamental microstructural unit, and concluded that the most likely cause of permeability changes as detected by Fernandez & Quigley (1988) was flocculation of particles. Mesri & Olson (1971b) hypothesised that high water salinity and/or low dielectric constant of the pore fluid causes the contraction of aggregates of clay particles, consequently decreasing the volume of the pores within the aggregates (*intra-aggregate* or *micro-voids*) and increasing the volume of voids between the aggregates (*inter-aggregate* or *macro-voids*). The increase of macro-void size could then be the dominant mechanism explaining the increase in permeability with salinity. Although an explicit hierarchy (*aggregates against clusters*) is not introduced in these different works, from Yong (1999) it follows that aggregates are made of many clusters of particles.

Manuscript received 29 February 2012; revised manuscript accepted 12 October 2012.
Discussion on this paper closes on 1 August 2013, for further details see p. ii.
* Department of Structural, Geotechnical and Building Engineering, Politecnico di Torino, Italy.
† Department of Geotechnical Engineering and Geosciences, Universitat Politècnica de Catalunya, Barcelona, Spain.
‡ Department of Structural Engineering, Politecnico di Milano, Milano, Italy.

The impact of aggregated fabric on the hydro-mechanical behaviour of compacted active clays, and jointly how this fabric is influenced by stress and suction changes, is well documented in unsaturated conditions (Romero *et al.*, 2011; Della Vecchia *et al.*, 2012). For instance, Lloret *et al.* (2003) performed an experimental study on bentonite samples compacted at different dry densities: by investigating both the pore size distribution and the water retention properties, they evidenced the advantages of modelling the microstructure of the soil through a double-porosity framework to reproduce the soil behaviour correctly.

The aim of the present paper is twofold. First, it aims at evaluating the effects of salinity changes on the fabric of compacted bentonite samples exposed to saline solutions of sodium chloride (NaCl) and calcium chloride ($CaCl_2$) ranging from null solute concentration to nearly saturated conditions. This evaluation is done by considering changes in the size of the aggregates, documented by environmental scanning electron microscopy (ESEM) photographs, and the associated changes in the size of the pore network, as measured by mercury intrusion porosimetry (MIP) tests. Experimental observations actually suggest the existence of a double-structure arrangement, which evolves upon chemical changes, and allow the introduction of a double-structure conceptual model, based on the framework proposed by Gens & Alonso (1992). Such a conceptual model foresees that the chemo-hydro-mechanical behaviour of compacted active clays upon chemical changes is governed by the interaction of two structural levels, one being related to the aggregates and their internal pore network and the other to the pore space between them. Simple laws and parameters used to give a mathematical form to the conceptual model are calibrated in a natural way using direct experimental information. For the particular case of the mass exchange terms, the interpretation of MIP results is used.

Second, the paper aims at verifying whether the double-structure model, and the way it was characterised, is actually consistent with the measured volumetric response of compacted active clays upon chemical changes. This check is done by using the conceptual model and the parameters defined in the first part to simulate a salt diffusion test, performed under well-controlled chemo-mechanical boundary value conditions. The simulation accounts for coupled transport phenomena, and handles the effects of the double structure on hydraulic processes according to the conceptual scheme of Gerke & van Genuchten (1993a). While aiming at contributing to more accurate reproduction of chemo-hydro-mechanical processes in structured materials, to be used for field geoenvironmental cases, the model also complements the experimental information of evolutionary processes at the local scale that are beyond the measurable scale of the macroscopic oedometer test performed. Thus the model should be also considered as a simulation-aided technique to better interpret and exploit the information provided by the phenomenological boundary value test.

For the sake of simplicity it was assumed that within the conditions explored during the tests, and reproduced by the model, cation exchange phenomena did not lead to relevant deformations. In order to make the model more compliant with formulations used in soil mechanics, chemical species and concentration changes were expressed in terms of variations of osmotic suction.

AN INSIGHT INTO MICROSTRUCTURAL CHANGES INDUCED BY CHEMICAL EFFECTS

The double structure of compacted active clays has been documented by several authors (e.g. Pusch, 1982; Atabek *et al.*, 1991; Lloret *et al.*, 2003; Musso *et al.*, 2003; Castellanos *et al.*, 2008; Romero *et al.*, 2011): particles of compacted active clays organise into aggregates, and pores within the aggregates are generally smaller than the pores between the aggregates.

In the present work, MIP tests and ESEM photomicrographs were performed to characterise the structure of samples of a compacted active clay (FEBEX bentonite) saturated with different saline solutions, so to provide information about the effects of chemical changes on the structural arrangement. Hydraulic conductivity measurements were also interpreted in the light of possible micro- and macroporosity changes.

FEBEX is a natural mixed bentonite (Cortijo de Archidona deposit, Almería, south-eastern Spain), proposed as an engineered barrier for radioactive waste disposal (ENRESA, 2000). It has a very high content of montmorillonite (around 90%), with small quantities of quartz, plagioclase, cristobalite, K-feldspars, trydimite and calcite. Table 1 summarises the main properties of the material.

Samples were prepared statically compacting the bentonite powder at a hygroscopic water content $w = 12\%$ (at a relative humidity of 50%), imposing an initial dry density $\rho_d = 1{\cdot}65$ Mg/m^3(void ratio $e = 0{\cdot}64$ and degree of saturation $S_r = 51\%$). Samples were subsequently loaded at constant water content up to a total vertical stress of 200 kPa, and then saturated with different saline solutions under oedometer conditions at constant vertical stress. All initially overconsolidated samples swelled upon saturation, although to different extents, depending on the solution used: so the overall final void ratios at which the microscopic analyses were performed are higher than the initial as-compacted one.

Effects detected by ESEM photomicrographs

ESEM photomicrographs were taken at different saturation conditions (as in Castellanos *et al.*, 2006), to visualise microfabric changes associated with different environmental conditions, and particularly with variations in the salinity of the pore fluid (Fig. 1). Aggregates with a size of around 100 μm, surrounded by macro-voids of comparable size, are clearly evident in the as-compacted state (Fig. 1(a)). Upon saturation, aggregates swell, reducing the volume of macro-voids between aggregates. Test results proved that the extent of aggregate swelling is noticeably influenced by the salinity of the pore fluid, since their size progressively increases from the hygroscopic state to that at saturation with 0·5 mol/l sodium chloride solution (Fig. 1(b)), and finally to the state induced by saturation with distilled water (Fig. 1(c)). In this last case, aggregates swell to such an extent that they start to merge.

Table 1. Properties of the bentonite used in the study*

Property	Value
Mineralogy	Montmorillonite (90 ± 3%)
Cation exchange complex: meq/100 g	Ca^{2+} (38%): 43
	Na^{+} (23%): 25
	Total CEC: 102
Liquid limit, w_L: %	102 ± 4
Plastic limit, w_P: %	53
Density of solids, ρ_S: Mg/m^3	2·70 ± 0·04
Particles < 2 μm: %	>85%
Specific surface, S_S: m^2/g	725 (total)
	65 (external)

* Lloret *et al.* (2003); Musso *et al.* (2003); Villar *et al.* (2005).

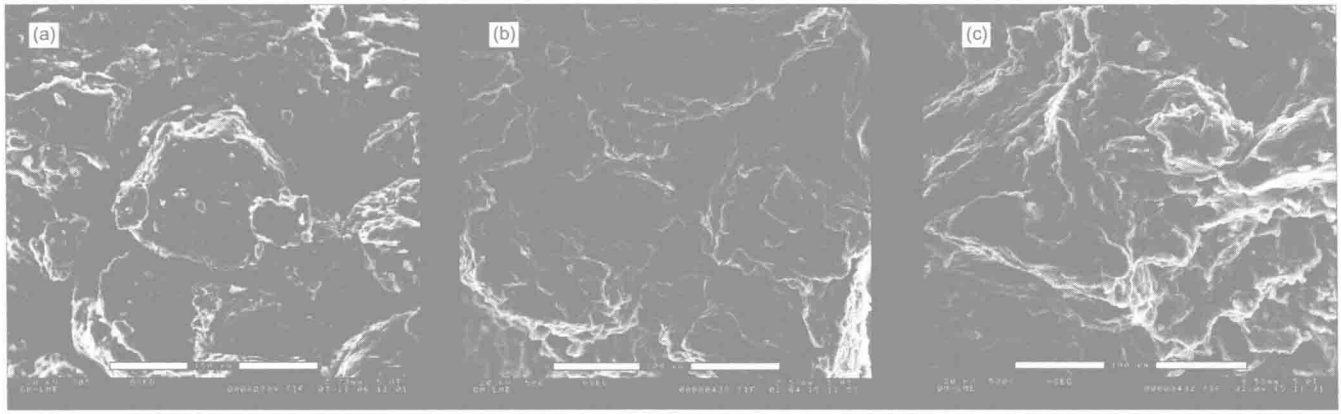

Fig. 1. ESEM pictures of statically compacted FEBEX samples (dry density 1·65 Mg/m^3): (a) as-compacted at hygroscopic water content, (b) after saturation with 0·5 mol/l sodium chloride solution; (c) after saturation with distilled water. Black bar is 150 μm in (a) and 100 μm in (b) and (c)

Effects detected by pore size distribution analyses

ESEM pictures testify that decreasing pore fluid salinities lead not only to greater aggregate size, but also to a progressive reduction of the size of macro-voids. Quantification of the evolution of the pore size was attempted by performing MIP on freeze-dried samples (Delage *et al.*, 1982) so as to obtain pore size distributions (PSDs) at different pore fluid concentrations. The device used was a Micromeritics-Autopore IV, which makes possible the intrusion of pore throats from 6 nm to 400 μm.

PSDs of the as-compacted sample at hygroscopic water content and of the overconsolidated samples saturated with different saline solutions are presented in Fig. 2. The PSD has been calculated as $-\Delta e/\Delta \log x$, where e is the intruded void ratio for each entrance pore diameter x: thus the area subtended by the PSD function represents the present void ratio. A consistent effect of salinisation on the PSD can be appreciated. The as-compacted sample shows a bimodal pore size distribution, with a peak at around 20 nm and another at around 20 μm. Upon saturation with highly saline solutions (5·5 mol/l), the overall void ratio increased from the original value $e = 0{\cdot}64$ to $e = 0{\cdot}75$ for the sodium chloride solution and to $e = 0{\cdot}74$ for the calcium chloride solution. The shape of the PSD suggests that the porosity increase upon saturation is partially related to a higher density of pores whose sizes are greater than approximately 20 μm. At lower salinities the density of this class of large pores progressively reduces, whereas the density of pores with sizes ranging from 100 nm to 10 μm increases significantly. The distribution of PSD function for salinities lower than 0·5 mol/l is such that a new peak emerges at a size of about 1000 nm, which is associated with the swelling of aggregates on saturation with a low-salinity fluid.

Measurements confirm that the microstructural effects of chemical changes on compacted soils are different from what could be expected for suspensions of active clays, where according to theories such as that of Derjaguin–Landau–Verweyd–Overbeek (e.g. Mitchell & Soga, 2005) a uniform pore size is expected, reducing upon an increase of salinity because of decreasing repulsion between single particles. MIP evidence also seems in contrast with externally measured deformations, since experimental studies record that salinisation induces an overall shrinkage of soil samples (e.g. Barbour & Fredlund, 1989; Di Maio, 1996; Gajo & Maines, 2007). A conceptual interpretation in terms of double porosity can help to explain these apparently opposite effects, provided the consequences of salt concentration changes for the micro-voids are different from the consequences of the same changes for macro-voids.

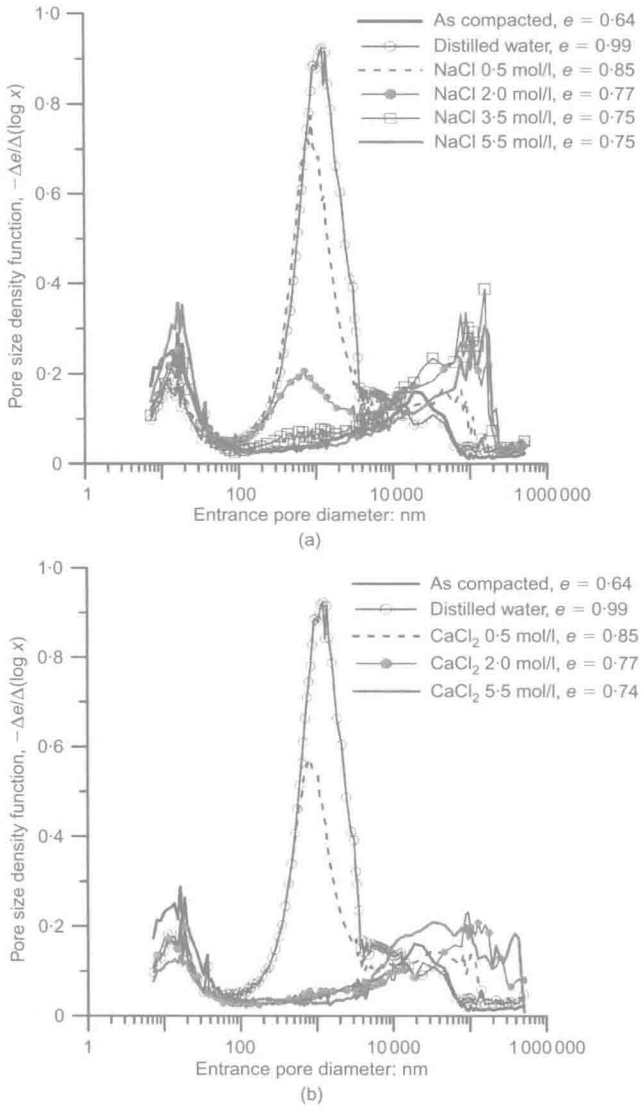

Fig. 2. MIP pore size distributions of compacted samples saturated with: (a) sodium chloride (NaCl) solution; (b) calcium chloride ($CaCl_2$) solution

Relation between salt concentration and microstructural void ratio

To put forward a quantitative interpretation in terms of double porosity, the (global) void ratio e can be split into

two components, the microstructural void ratio e_m and the macrostructural void ratio e_M, according to

$$e = e_m + e_M = \frac{V_{vm}}{V_s} + \frac{V_{vM}}{V_s} \quad (1)$$

where V_{vm} is the volume occupied by micro-voids, V_{vM} is the volume occupied by macro-voids, and V_s is the volume of solids.

It was decided to discriminate between e_m and e_M on the basis of the MIP measurements presented in the previous section, by defining a delimiting pore size that made it possible to account for the evolving size of the aggregates during chemo-hydraulic processes. As explained in Della Vecchia (2009) and Romero *et al.* (2011), the working hypothesis is that pores belonging to the microstructure can increase their size up to a limit, corresponding to the minimum size of the pores belonging to the macrostructure. So the delimiting pore size is at the same time an upper bound for the intra-aggregate porosity and a lower bound for the inter-aggregate porosity. It can be determined from MIP data referring to the condition that promotes the most significant swelling of the aggregates (in this case saturation with distilled water), since the intra-aggregate pores will have their maximum size and the inter-aggregate pores their minimum size. The delimiting pore size was then chosen in correspondence with the dominant maximum peak of the PSD of the distilled water saturated sample. According to this hypothesis, micro-voids are characterised by pores with a diameter lower than 1000 nm and macro-voids by pores with a diameter greater than 1000 nm (Fig. 2). For each solute type and salt concentration, V_{vm} was then evaluated as the volume occupied by voids whose entrance pore sizes are lower than 1000 nm. The corresponding values of e_m and e_M were obtained by equation (1).

According to the defined phenomenological framework, the sizes of the aggregates and micro-voids are different from the sizes of clusters and intra-cluster voids used in other works (e.g. Hueckel *et al.*, 1997). Since intra-cluster voids are saturated by externally adsorbed water, their size is below what is measured with the MIP technique, while the size of the elements here defined is based on the observations collected through ESEM and MIP analyses previously discussed, that is, on a broader scale. A single aggregate is regarded as composed of several clusters, so that, in accordance with Terzaghi (1956) 'the range of influence of the osmotic forces does not extend beyond the boundaries of each of the clay clusters which are scattered throughout the aggregate, but within these boundaries their influence is decisive.'

PSD changes induced by sodium chloride and calcium chloride solutions on FEBEX samples appeared comparable (Figs 2(a) and 2(b)), so that a working hypothesis that cation exchange did not induce relevant deformations was introduced, and osmotic suction π was used as a constitutive variable. According to the van't Hoff expression, osmotic suction can be written as

$$\pi = icRT \quad (2)$$

where i is the number of constituents into which the molecule separates upon dissolution ($i = 2$ for sodium chloride and $i = 3$ for calcium chloride), c is the molar concentration, R is the universal gas constant, and T is the absolute temperature.

Figure 3 shows the evolution of the microstructural void ratio e_m as a function of the osmotic suction π. Experimental data are reasonably reproduced by the expression

$$d\varepsilon_{vol}^m = \beta e^{-\alpha\pi_m} d\pi_m \quad (3)$$

being

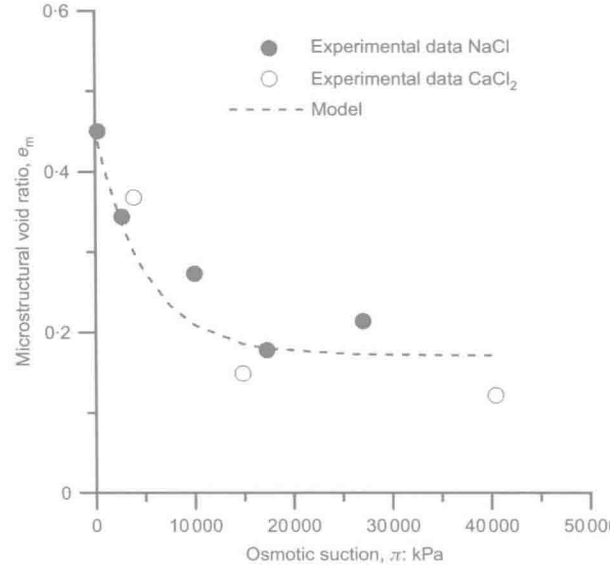

Fig. 3. Dependence of microstructural void ratio e_m on osmotic suction

$$d\varepsilon_{vol}^m = -\frac{de_m}{1+e} \quad (4)$$

where π_m is the osmotic suction of the solute in the micro-voids, ε_{vol}^m is the volumetric strain of the microstructure, and α and β are constitutive parameters of the material. The evolution of ε_{vol}^m as described by equation (3) is qualitatively similar to the predictions of the DDL theories (although the delimiting pore size of 1000 nm is well beyond the typical thickness of a double layer), and recalls the proposal of Alonso *et al.* (1994), originally formulated in terms of total suction instead of osmotic suction. Parameter calibration of equation (3) has been performed on the basis of the experimental data presented in Fig. 3, obtaining $\beta = 3{\cdot}2 \times 10^{-5}$ kPa^{-1} and $\alpha = 2{\cdot}0 \times 10^{-4}$ kPa^{-1}.

Effects of osmotic suction on hydraulic conductivity

As previously discussed, the hydraulic conductivity of bentonite samples is strongly influenced by the saline concentration of the wetting fluid (e.g. Mesri & Olson, 1971b; Calvello *et al.*, 2005; Gajo & Maines, 2007). Experimental data for the hydraulic conductivity of compacted and reconstituted FEBEX samples, saturated with saline solutions at different concentrations, are shown in Fig. 4. These values were determined by interpreting oedometer tests with Terzaghi's one-dimensional consolidation theory. Reconstituted samples were prepared by mixing FEBEX powder with saline solutions at the relevant concentration c (0·05 mol/l sodium chloride, 0·10 mol/l sodium chloride, 5·50 mol/l sodium chloride). The water content at which samples were prepared was equal to $1{\cdot}2w_L(c)$, where $w_L(c)$ is the liquid limit of the soil at a given concentration c. The pertinent values were $w_L = 105\%$ for $c = 0{\cdot}05$ mol/l, $w_L = 90\%$ for $c = 0{\cdot}10$ mol/l, and $w_L = 52\%$ for $c = 5{\cdot}5$ mol/l.

As expected, the hydraulic conductivity K increases with the global void ratio e. At a given e, K is greater the greater the saline concentration c (or the osmotic suction π). These results are in line with MIP and ESEM evidence, since the increase of the size of the inter-aggregate voids, related to higher osmotic suction, can explain the higher hydraulic conductivity. MIP evidence and the increase of K with osmotic suction (interestingly occurring also in the reconstituted samples) confirm the hypothesis of Mesri & Olson

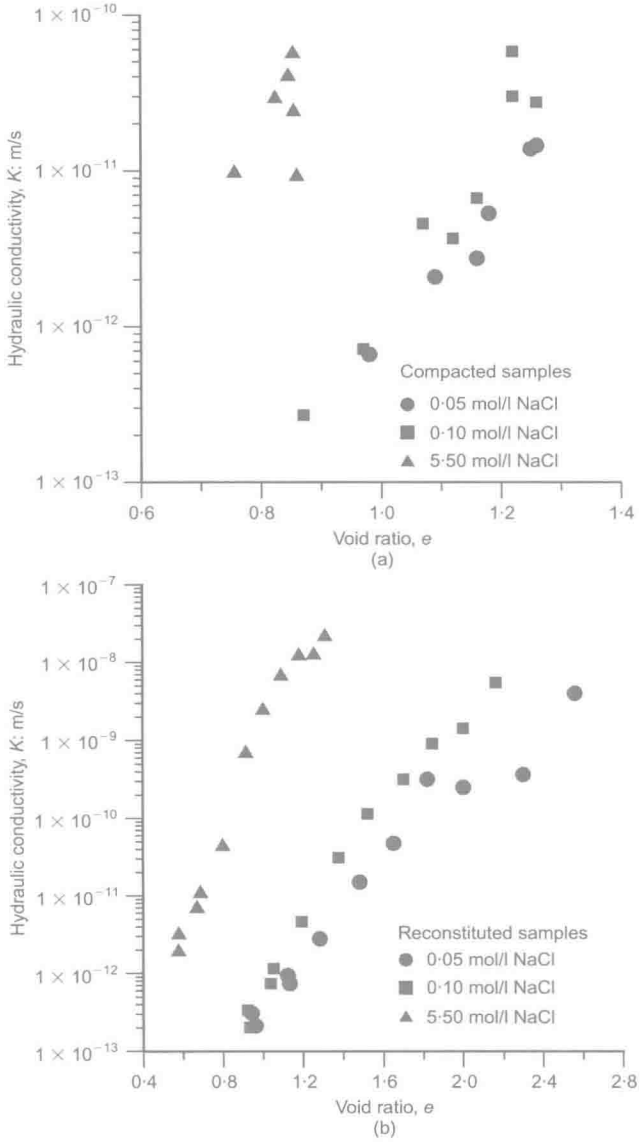

Fig. 4. Dependence of hydraulic conductivity of (a) compacted and (b) reconstituted FEBEX samples on void ratio for different salt concentrations

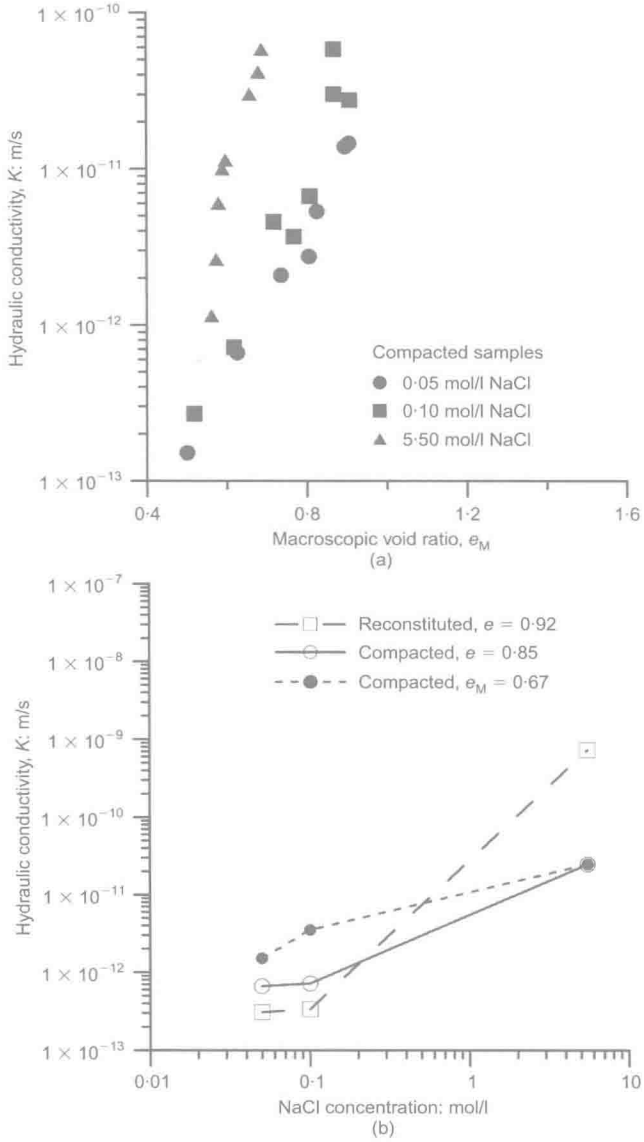

Fig. 5. Relationship between hydraulic conductivity of FEBEX samples and: (a) macrostructural void ratio e_M for different salt concentrations; (b) salt concentration at the same void ratios

(1971b) concerning the consequences of the contraction of the aggregates for permeability.

The relationship between the hydraulic conductivity and the macroscopic void ratio e_M, determined as $e_M = e - e_m$, is shown in Fig. 5(a). The microstructural void ratio e_m was assumed not to depend on the vertical effective stress applied during the test. The difference between the conductivities at different π reduces if e_M is used instead of e as a reference state variable (Fig. 5(b)).

EFFECTS OF DOUBLE STRUCTURE ON CHEMO-MECHANICAL BEHAVIOUR

Chemically induced volumetric strains

Castellanos *et al.* (2008) reported experimental data concerning the effects of salinity on the mechanical behaviour of saturated compacted FEBEX bentonite ($\rho_d = 1{\cdot}65$ Mg/m^3). Swelling tests had been performed in a conventional oedometer, soaking unsaturated samples with sodium chloride and calcium chloride solutions under a vertical total stress of 500 kPa. The results of these swelling tests provided the basis for the characterisation of the overall chemo-mechanical volumetric behaviour of compacted FEBEX bentonite, detailed in the following.

It is here assumed that the strain induced by a change of osmotic suction ($\pi_1 - \pi_0$) in a saturated sample is equal to the difference between the strains induced by saturation with fluids having osmotic suctions π_1 and π_0. The overall volumetric strain due to osmotic suction changes with respect to distilled water is thus $\varepsilon_{vol}(\pi) = \varepsilon_{sw}(\pi) - \varepsilon_{sw}(0)$, where $\varepsilon_{sw}(0)$ and $\varepsilon_{sw}(\pi)$ are the swelling strains obtained when the osmotic suction at saturation is 0 and π respectively. The experimental results organised this way are shown in Fig. 6 (closed and open symbols); the overall sensitivity to osmotic suction changes is much more pronounced at low suctions.

Interpretation of chemically induced strains in light of a double structure formulation

According to equation (1), the overall volumetric strain is the sum of the volumetric strains associated with the micro-voids and the macro-voids. Characterisation of the double-structure medium could in theory be pursued by measuring

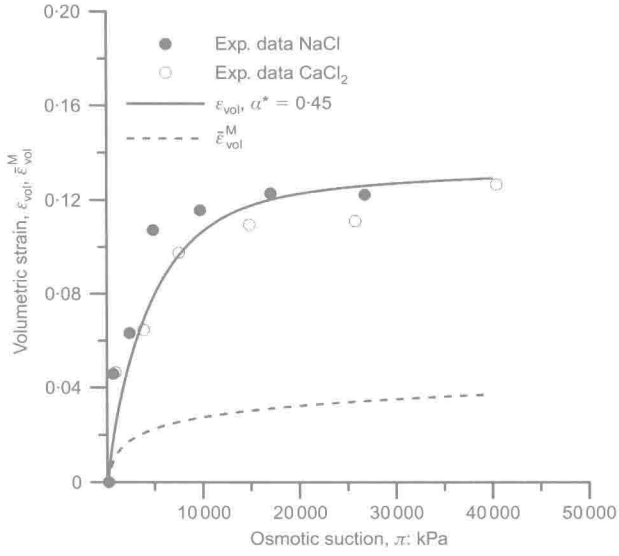

Fig. 6. Volumetric strains due to salinisation with sodium chloride (NaCl) and calcium chloride ($CaCl_2$)

the volumetric strains of the two different domains independently. In practice, this is not feasible; from external measurements it is not possible to discriminate the two different contributions. For example, during a water dilution process, both the aggregates and the soil sample swell: as a result, the volume change of the macro-voids is the difference between the volume change of the sample and that of the aggregates (micro-voids). In the limiting case of a constant-volume test, macropore volume reduction is equal and opposite to aggregate volume expansion. As a dual aspect, only a fraction α^* of aggregate strain contributes to the overall strain. The remaining fraction $(1-\alpha^*)$ results in a reduction of the macroporosity (macro-void invasion).

In the light of the previous considerations, it is convenient to express the overall volumetric strain

$$d\varepsilon_{vol} = d\bar{\varepsilon}^{M}_{vol} + \alpha^* d\varepsilon^{m}_{vol} \tag{5}$$

where $d\bar{\varepsilon}^{M}_{vol}$ is the volumetric strain that the macroporosity would experience at constant aggregate size. α^* can thus be interpreted as the fraction of microstructural volumetric strain that does not contribute to macropore invasion.

From a practical point of view, it is convenient to characterise the relationship between $d\bar{\varepsilon}^{M}_{vol}$ and $d\pi$ over a range of concentration where microporosity is not influenced by osmotic suction changes. Characterisation of the microstructural strains presented in equation (3) and Fig. 3 suggests that microstructural strains are negligible when π increases from 15 MPa to 40 MPa, so that characterisation of the dependence of $d\bar{\varepsilon}^{M}_{vol}$ on π could be obtained in this range.

Under the assumption of oedometer conditions and constant vertical load, the variation of volumetric strain can be written as

$$d\bar{\varepsilon}^{M}_{vol} = m_\pi d\pi_M \tag{6}$$

where m_π is the constitutive parameter that takes into account the compliance of the soil against osmotic suction variations. To account for non-linearity of the mechanical response, volumetric compliance has been imposed to depend on the current osmotic suction

$$m_\pi = \frac{k_\pi}{\pi_M} \tag{7}$$

where k_π is a constant.

The value of k_π can thus be calibrated on the slope of the $\varepsilon_{vol}-\log\pi$ data in the high-π range; as for the compacted samples, a value $k_\pi = 0{\cdot}015$ was obtained as an average value on a wider set of data available in Castellanos *et al.* (2008). In Fig. 6, the $\bar{\varepsilon}^{M}_{vol}-\pi$ curve predicted by the model is depicted by the dotted line. The difference $\alpha^*\varepsilon^{m}_{vol} = \varepsilon_{vol} - \bar{\varepsilon}^{M}_{vol}$ is the fraction of microstructural swelling that contributes to the volume change of the sample.

Following Gens & Alonso (1992), it is reasonable to assume that α^* is a function of density and current stress level. If it is also assumed that the microstructural strain depends only on changes in the driving variables (i.e. in this case the osmotic suction acting within the micro-voids), once the values of k_π, α and β are known, the value of α^* for the given applied stress and initial density can be calibrated based on experimental data at low values of π. The continuous line in Fig. 6 was obtained with equation (5), using $\alpha^* = 0{\cdot}45$. An overall good reproduction of experimental data is evident.

EFFECTS OF DOUBLE STRUCTURE ON HYDRO-CHEMICAL TRANSPORT

The mechanical characterisation presented in the previous sections was pursued under well-equilibrated conditions. Stationary conditions of the deformation before experimental analyses were assumed, so as to assume that water pressure and osmotic suction in the inter-aggregate and in the intra-aggregate domain were in equilibrium.

Engineering structures are exposed to transient flux conditions, which in a double-porosity medium can easily lead to disequilibrium between the two structural levels. Under varying chemical and hydraulic conditions, a comprehensive analysis of deformation processes must then take into account the overall transport of water and salt in the medium, and how mass is exchanged between the micro- and macro-domains.

In the following, transport phenomena are modelled considering the inter-aggregate and the intra-aggregate domains as homogeneous media with different hydraulic and solute transport properties (Barrenblatt *et al.*, 1960; Warren & Root, 1963; Wilson & Aifantis, 1981). The dual-porosity medium is considered to be a superposition of these two systems over the same volume (Gerke & van Genuchten, 1993a). Microporosity ϕ_m and macroporosity ϕ_M are then defined as the volume of the corresponding pores divided by the overall volume V_{tot}.

$$\phi_m = \frac{V_{vm}}{V_{tot}} = \frac{e_m}{1+e}$$
$$\phi_M = \frac{V_{vM}}{V_{tot}} = \frac{e_M}{1+e} \tag{8}$$

At each point, the hydraulic and osmotic potentials in the two continua may be different, so that salt and water can be exchanged between them. Deformation in the two domains follows from equations (3), (5) and (6).

Mass fluxes occurring completely within the microporosity are hypothesised to be negligible, so that mass of water and of solute can move from the intra-aggregate pores only towards (or from) the macroporosity. The mass balance of water for the microporosity (m) and for the macroporosity (M) is then given by

$$\frac{\partial \rho_w \phi_m}{\partial t} - q^{EX}_w = 0 \tag{9a}$$

$$\frac{\partial \rho_w \phi_M}{\partial t} + \nabla \cdot (\rho_w v) + q^{EX}_w = 0 \tag{9b}$$

where ρ_w is the density of water, $\boldsymbol{v}$ is the volumetric flow of water relative to the solid skeleton, and q_w^{EX} is the water mass transfer term between micro- and macropores.

Similarly, the mass balance equations for the solute are

$$\frac{\partial c_m \phi_m}{\partial t} - q_s^{EX} = 0 \tag{10a}$$

$$\frac{\partial c_M \phi_M}{\partial t} + \nabla \cdot (\boldsymbol{j}) + q_s^{EX} = 0 \tag{10b}$$

where c_m and c_M are the saline concentrations in the micro- and macropores, $\boldsymbol{j}$ is the total flux of solute mass, and q_s^{EX} is the salt mass transfer term. Both q_s^{EX} and q_w^{EX} are positive when the mass exchanged is directed towards the microporosity. The exchange and transport terms used are briefly discussed in the following.

Mass exchange terms

The water and solute mass transfer terms are related to each other, being transfer of solute due to both advection and diffusion contributions. From equation (9a) with incompressible water and equation (10a) it follows that

$$\frac{\partial \phi_m}{\partial t} - \frac{q_w^{EX}}{\rho_w} = 0 \tag{11a}$$

$$\phi_m \frac{\partial c_m}{\partial t} + c_m \frac{\partial \phi_m}{\partial t} - q_s^{EX} = 0 \tag{11b}$$

and thus for consistency

$$q_w^{EX} = \frac{\rho_w q_s^{EX}}{c_m} - \frac{\rho_w \phi_m}{c_m} \frac{\partial c_m}{\partial t} \tag{12}$$

It is generally assumed that mass exchange terms are proportional to the difference between the driving potentials in the two structural levels (e.g. Gerke & van Genuchten, 1993b). In this work it was assumed that salt mass transfer is a diffusion-like phenomenon, and q_s^{EX} was defined as

$$q_s^{EX} = \chi(c_M - c_m) \tag{13}$$

where χ is a first-order transfer coefficient.

In the study of flow in saturated media with limited deformability, the first-order transfer coefficient χ is often expressed as a function of the hydraulic conductivity K (Warren & Root, 1963), through a relationship of the form

$$\chi = \chi^* \cdot K \tag{14}$$

where χ^* is a function of the geometry of the aggregates.

Figure 7 presents a conceptual scheme of the transport and exchange mechanism for different aggregate sizes (larger aggregates enhance mass exchanges between the two domains, as shown in Fig. 7(b), reducing the inter-aggregate pores and consequently the transport across the macrostructural domain). P_M and p_m represent the water pressure in the macro- and micro-structural domain, respectively.

Gerke & van Genuchten (1993a) extended the formulation to the case of unsaturated porous media, associating K to the permeability of the microporosity domain, which is a function of the degree of saturation. This observation was extended to the present case by considering that concentration changes affect the size of the microporosity domain, so that concentration was used instead of the degree of saturation. According to Romero *et al.* (1999), relative permeability is related to the size and distribution of the interconnected pores, and thus predictive equations based on PSDs make it possible to reflect this dependence. Starting

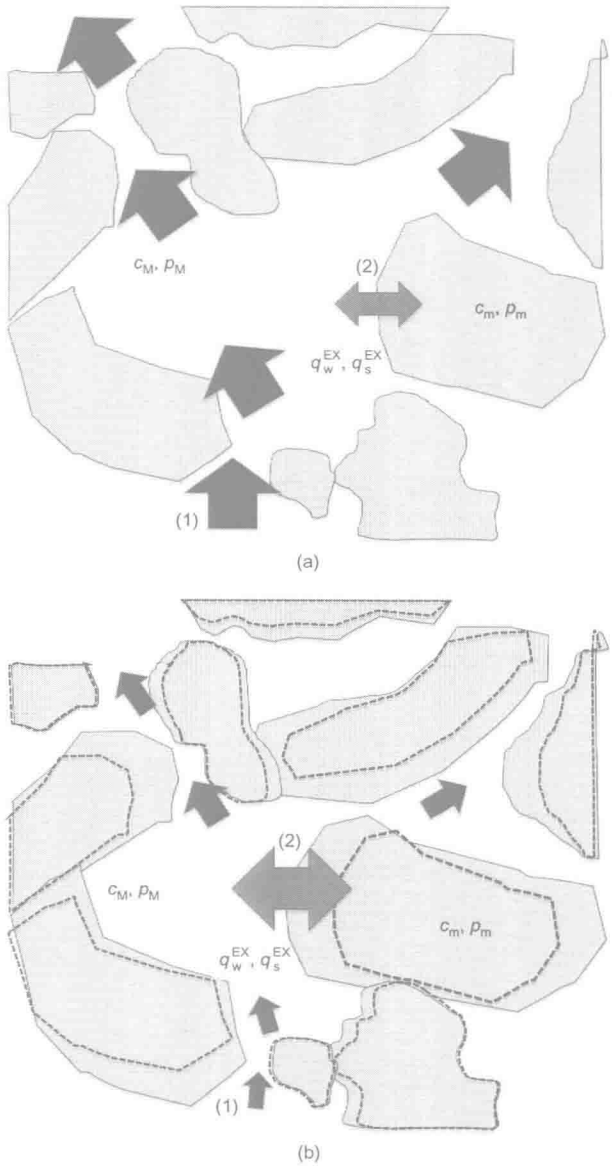

Fig. 7. Conceptual scheme of transport mechanism: (1) mass fluxes within inter-aggregate space; (2) mass exchange between inter-aggregate and intra-aggregate spaces. (a) High-suction range: aggregates have smaller dimensions; larger inter-aggregate pores enhance transport across macroscopic domain. (b) Low-suction range: larger aggregates enhance mass exchange between the two domains

from Leong & Rahardjo (1997), the role of evolving aggregates in equation (14) can be taken into account as

$$K \propto -\int_0^{x_{lim}} x^2 \frac{\partial e}{\partial x} dx = f(c) \tag{15}$$

where x_{lim} is the diameter representing the threshold between microporosity and macroporosity, which earlier was set equal to 1000 nm, and $f(c)$ is a function of salt concentration. The ratio $f(c)/f(c=0)$ was evaluated for all the available PSDs, and its evolution is presented in Fig. 8. A possible mathematical equation for the transfer coefficient χ is then

$$\chi = \hat{\alpha} \exp(-\hat{\gamma} c_M) \tag{16}$$

where $\hat{\alpha}$ and $\hat{\gamma}$ are two parameters to be calibrated on the phenomenological response of the material.

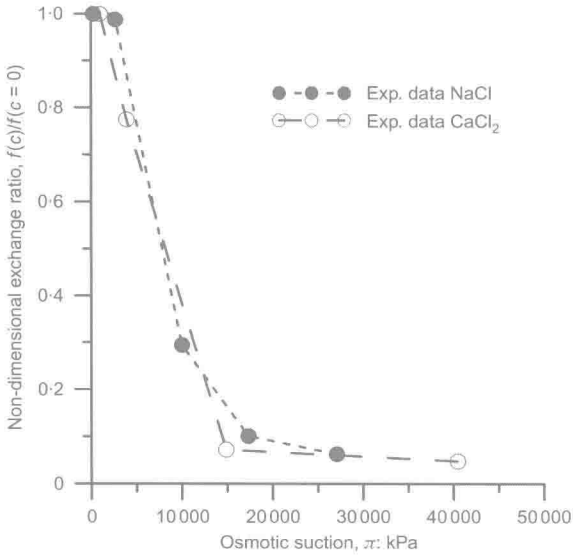

Fig. 8. Normalisation of transfer term at given concentration with respect to null concentration condition. Transfer terms are hypothesised to depend on permeability of microstructure, reconstructed on MIP measurements

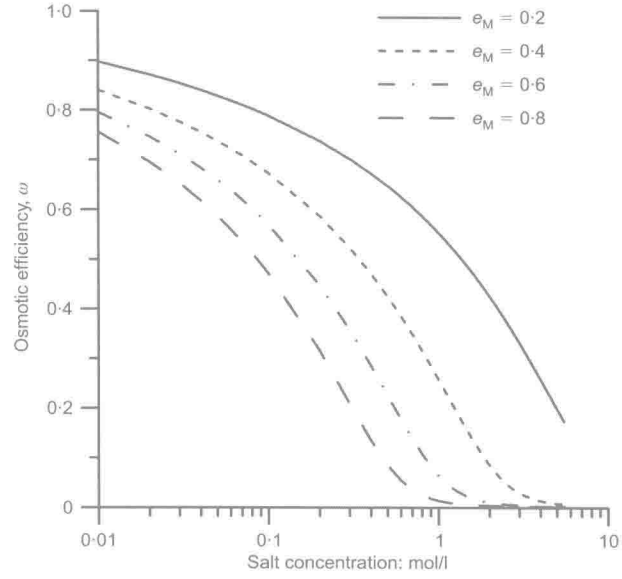

Fig. 9. Dependence of osmotic efficiency ω on salt concentration (two monovalent species) and on macroscopic void ratio for FEBEX bentonite. Interpretation based on data of Bresler (1973), using external specific surface of soil

Fluxes of water and solute

Water and salt flow through the macrostructure was formulated following the theory of irreversible thermodynamics, introducing a number of coupled flows (e.g. Yeung & Mitchell, 1993; Manassero & Dominijanni, 2003; Lu *et al.*, 2004). Neglecting the presence of electrical gradients, water flow is driven by the gradients of both hydraulic and osmotic potentials

$$\boldsymbol{v} = -\frac{K_{\mathrm{M}}}{\rho_{\mathrm{w}}\boldsymbol{g}}\nabla(p_{\mathrm{M}} + \rho_{\mathrm{w}}\boldsymbol{g}z) + \frac{K_{\pi}}{\rho_{\mathrm{w}}\boldsymbol{g}}\nabla(\pi_{\mathrm{M}}) \tag{17}$$

where $\boldsymbol{g}$ is gravitational acceleration, K_{M} is macrostructural hydraulic conductivity, and K_{π} is osmotic permeability. The latter is related to the former by the coefficient of osmotic efficiency, ω (e.g. Mitchell & Soga, 2005), so that $K_{\pi} = \omega K_{\mathrm{M}}$.

The experimental data of Bresler (1973) concerning the dependence of osmotic efficiency ω on salt concentration in the macro-voids c_{M} were expressed through a suitable fitting expression

$$\log\omega = B - \arctan\left\{A\left[\log\left(10b\sqrt{c_{\mathrm{M}}}\right) + C\right]\right\} \tag{18}$$

where b is the half-distance between soil particles. If b is expressed in nm and c_{M} in normality (for dominant monovalent cations, equivalent to mol/l), it follows that $A = 5{\cdot}5$, $B = -1{\cdot}5$ and $C = -1{\cdot}3$ for salts with monovalent cations. Since in this work the osmotic flow is assumed to occur only through the macropores, b was estimated from the specific surface of the solid particle S_{S} and the void ratio of the macropores e_{M} (Mitchell & Soga, 2005) according to

$$b = \frac{1}{2}\frac{e_{\mathrm{M}}}{S_{\mathrm{S}}\rho_{\mathrm{S}}} \tag{19}$$

where ρ_{S} is the density of the solid particles; then b is here the average half-distance between aggregates. Fig. 9 shows the evolution of the osmotic coefficient as a function of salt concentration in the macropores, for different void ratios.

The salt flow in the macropores, $\boldsymbol{j}$, is due to both advection and diffusion. Neglecting the movement of the solid phase with respect to the reference configuration, it can be written as

$$\boldsymbol{j} = c_{\mathrm{M}}(1-\omega)\boldsymbol{v} - D_{\mathrm{M}}\nabla c_{\mathrm{M}} \tag{20}$$

where D_{M} is the effective diffusion coefficient, accounting for the effects of porosity, tortuosity, osmotic efficiency and retardation. In the following the term D_{M} will be expressed as $D_{\mathrm{M}} = (1-\omega)D_{\mathrm{M0}}$, where D_{M0} is the effective diffusion coefficient in the absence of osmotic effects.

APPLICATION OF THE FRAMEWORK

The double-porosity framework was applied to simulate a salt diffusion test run in an oedometer at constant vertical stress. The aim of the simulation was to verify the capabilities of the framework in capturing the main features of the mechanical and transport processes induced by desalinisation and subsequent salinisation. The simulated test was performed in a modified oedometer cell, which connects each porous stone with a reservoir aimed at hosting small quantities of solution (Fig. 10). Concentration evolution in the reservoirs was estimated on the basis of electrical conductivity measurements, by converting electrical conductivity into equivalent concentrations of sodium chloride (e.g. Shackelford *et al.*, 1999).

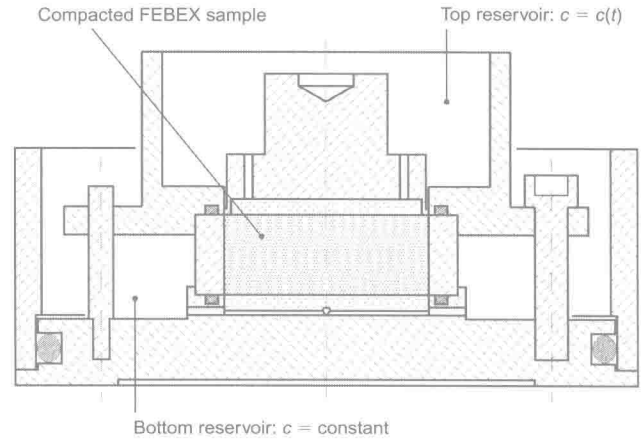

Fig. 10. Modified oedometer cell used for desalinisation–salinisation test

A sample 10·5 mm high was prepared by statically compacting the FEBEX material to a dry density $\rho_d = 1{\cdot}68$ Mg/m^3 at hygroscopic water content $w = 12\%$. The sample was placed in the oedometer and loaded (total vertical stress $\sigma_v = 200$ kPa). Saturation was induced by pouring into the two reservoirs a 5·5 mol/l sodium chloride solution and letting the sample swell accordingly. Once strain equilibrium was achieved, the saline solution was removed from the bottom reservoir, and replaced with distilled water. To ensure constant concentration conditions, this operation was repeated daily. As a consequence of the induced water and salt fluxes, salt concentration diminished in the sample and in the upper reservoir. This was evidenced by chemo-mechanical swelling, and by a progressive drop of the electrical conductivity in the top reservoir. To compensate for the volume of water lost upon evaporation, the original volume of the solution in the reservoir was maintained constant by adding distilled water. Once swelling and electrical conductivity drop had stopped, the bottom reservoir was filled with a 5·5 mol/l sodium chloride solution to revert the process. The test lasted about 1 year.

Simulation of the test was performed by way of finite-element solution of the balance equations (equations (9) and (10)). One-dimensional parabolic elements for both the salt and water mass balances were used. The physical evidence adopted as a reference for the verification of the framework comprised the evolution of the vertical displacement and of the sodium chloride concentration in the top reservoir. As for the latter, the volume of the reservoir influences the concentration and transport of salt, so that to track concentration evolution the reservoir was also simulated as a porous medium with very high hydraulic conductivity and a diffusion coefficient equal to the free diffusion coefficient of sodium chloride in water ($D = 1{\cdot}9 \times 10^{-9}$ m^2/s). The porosity of the dummy porous medium was selected in order to have a volume of voids equal to the volume of the reservoir. At the contact between the reservoir and the sample, a no-jump condition in terms of the normal component of the total flux of the salt and water was imposed (Bear & Cheng, 2010). At the upper boundary of the reservoir a no-flux condition for both water and salt was imposed. The scheme of the media and boundary conditions introduced is given in Fig. 11.

Time zero of the simulation was the end of saturation. The initial total and microstructural void ratios were set equal to $e_0 = 0{\cdot}72$ (corresponding to the initial dry density) and $e_{m0} = 0{\cdot}17$ (according to the MIP interpretation of Fig. 3). Consequently, the macroscopic void ratio was calculated as $e_{M0} = e_0 - e_{m0} = 0{\cdot}55$. In both the microstructural and macrostructural domain, the initial chemical condition was $c_{m0} = c_{M0} = 5{\cdot}5$ mol/l, and atmospheric hydraulic pressure was imposed.

The parameter values used for the simulation are presented in Table 2. The hydraulic and mechanical parameters were directly derived from the analysis given in the previous sections, which refer to independent tests performed on the same material. This holds for: the hydraulic conductivity K_M (a constant average value for the porosity of interest was chosen; see Fig. 5); the parameters describing the evolution

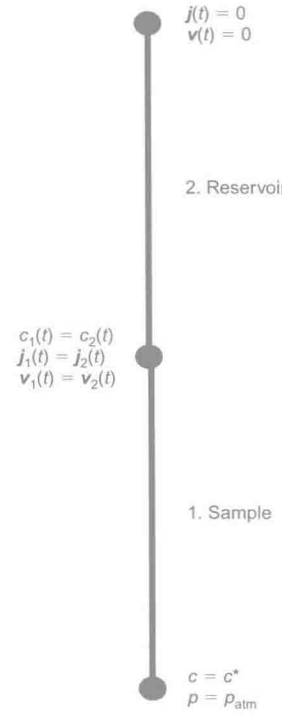

Fig. 11. Boundary condition for simulation of desalinisation–salinisation test

of the microstructural void ratio upon osmotic suction changes, α and β (Fig. 3 and equation (3)); the parameter describing the mechanical interaction between the micro- and macrostructure, α^* (Fig. 6 and equation (5)); and the compressibility of the macrostructure, k_π (Fig. 6 and equation (6)). The effective diffusion coefficient of the macrostructure, D_{M0}, was chosen according to literature data for this type of material and density (Bourg *et al.*, 2006), and the osmotic efficiency ω was set to depend on the macrostructural void ratio and concentration, as in equations (18) and (19). The parameters of the first-order transfer function (equation (16)), $\hat{\alpha}$ and $\hat{\gamma}$, were instead calibrated through back-analysis on the recorded displacement evolution along desalinisation.

Good agreement between the simulated and measured vertical displacements of the sample upon chemical cycling was obtained (Fig. 12). Consistent results were also obtained in terms of the time evolution of the measured and simulated salt concentrations in the upper reservoir (Fig. 13).

DISCUSSION

The results of the simulation can be used to outline the main effects imparted by the structural arrangement to the history of concentrations and strains.

The histories of vertical displacements and the salt concentration measured within the top reservoir appear to depend strongly on the direction of chemical loading. Both

Table 2. Parameters used in the simulation

Mechanical parameters				Transport parameters			
Microstructure compressibility: kPa^{-1}		Macrostructure logarithmic osmotic compliance, k_π	Interaction function, α^*	Hydraulic conductivity, k_M: m/s	Effective diffusion, D_{M0}: m^2/s	Transfer function	
α	β					$\hat{\alpha}$: s^{-1}	$\hat{\gamma}$: l/mol
$2{\cdot}0 \times 10^{-4}$	$3{\cdot}2 \times 10^{-5}$	0·015	0·45	5×10^{-12}	9×10^{-11}	0·8	8

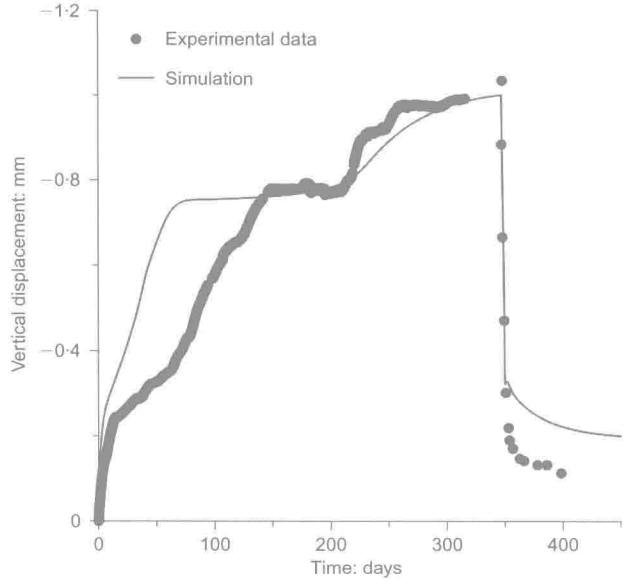

Fig. 12. History of vertical displacements during salinisation–desalinisation test (negative displacements mean sample swelling)

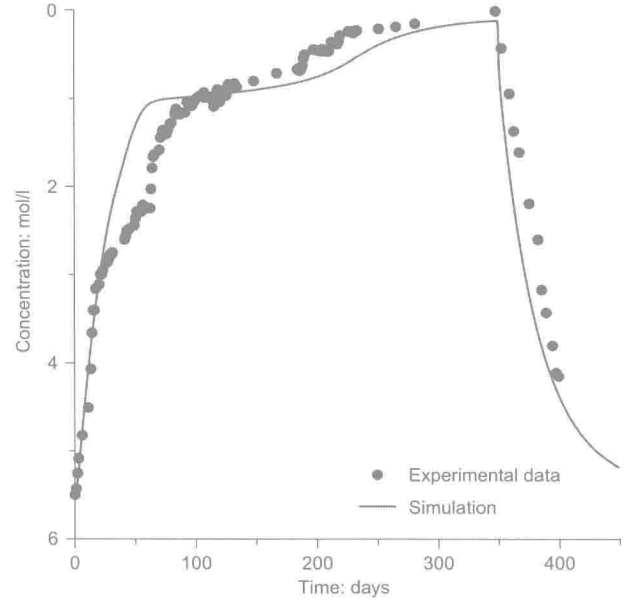

Fig. 13. History of sodium chloride concentration in upper (free) reservoir during salinisation–desalinisation test

deformations and concentration evolve more rapidly upon salinisation than upon desalinisation. This is especially evident for the history of deformations, with a difference in timescales of about 1/10. Similar evidence has been previously noted by several authors working on reconstituted specimens of different active clays (e.g. Barbour & Fredlund, 1989; Di Maio, 1996; Gajo & Maines, 2007). The fact that deformation proceeds quite continuously in a single stage during salinisation (shrinkage), and very discontinuously in different stages upon desalinisation (swelling), as shown in Fig. 12, is also remarkable. This aspect does not pertain to reconstituted soils, but is reported in previous experimental works on compacted FEBEX samples (Musso *et al.*, 2003). An analogous phenomenon has been documented by Rao & Thyagaraj (2007), who performed a series of tests on Indian active clay: specimens were prepared at different saline contents, compacted in unsaturated conditions and then saturated with distilled water under a small seating load. In their work, Rao & Thyagaraj (2007) identified two swelling stages for specimens prepared at low salt contents, and a third swelling stage emerging at longer times for specimens prepared at high salt content. Since the first swelling stage was due to the dissipation of matric suction, in Rao & Thyagaraj (2007) chemical swelling also occurs in a single stage when the initial salt content is low, and in two or more stages when the initial salt content is high.

Tracking of the deformation and of concentration induced by changes in the chemical boundary conditions is complicated by the several coupled transport processes, and by the different ways through which deformation can arise. Strains can arise because of osmotic suction changes (*osmotic consolidation* according to Barbour & Fredlund, 1989), and because of transient water flow caused by osmotic gradients (*osmotically induced consolidation* according to Barbour & Fredlund, 1989). Darcian flow associated with pore pressure variations, due to constrictions caused by the low permeability, and advective flow of the dissolved chemical further influence the deformation pattern (Kaczmarek & Hueckel, 1998; Peters & Smith, 2004).

Profiles of e_M and e_m at different times can be useful in understanding the evolution of the deformation process, and possibly the structural arrangement, as foreseen by the model. During the first 5 days, displacement progresses at a relatively fast rate (Fig. 12). The dominant role of e_M, whose increment is more noticeable in the lower part of the sample, although also appreciable at the upper side, is evidenced in Fig. 14(a). By contrast, the increase of e_m is limited to the bottom 3 mm of the sample (Fig. 14(b)). Taking as a reference the time interval between 2·5 and 5 days, the model predicts that, in the bottom part of the sample, e_M will progressively reduce while e_m increases; swelling aggregates are progressively invading the inter-aggregate porosity (as depicted in the conceptual scheme in Fig. 7(a)). The delayed deformation of the microstructure is associated with a slow release of salt towards the macrostructure, or, in other words, with values of microstructural osmotic suction remaining high, compared with the macrostructural values (Fig. 15). Indeed, since the salt concentration is initially high, the density of pores with size smaller than 1000 nm is low, and the transfer term χ is very small. Therefore, despite significant differences in suction, transfer of mass between the inter-aggregate and the intra-aggregate pore space occurs very slowly.

After 45 days, the macrostructural and microstructural suctions have about the same value (Fig. 15); this occurs while χ attains higher values, so that mass can be transferred more easily between the two structural levels. Between $t = 90$ days and $t = 240$ days, vertical displacements are about stable. Vertical displacements increase again significantly when t is greater than 240 days, clearly as a consequence of the higher sensitivity of both microstructural and macrostructural deformations to suction changes in the low-suction range (see Figs 3 and 6). Macroporosity is further invaded by swelling aggregates, and e_M globally reduces to values smaller than the initial ones (Fig. 14). Also, the salt concentration in the upper reservoir first attains a quasi-constant value and then starts to increase again (after approximately 200 days; Fig. 12). In the light of the hypothesis concerning the mass transfer coefficient, the increase in concentration occurring after 200 days could correspond to an easier release of mass from the microporosity to the macroporosity, and then from the latter to the reservoir (refer to the conceptual scheme of Fig. 7).

According to the analysis, hydraulic pressure within the macrostructure is not constant in space and time (Fig. 16), but nevertheless remains limited between −20 kPa and